Inorganic Chemistry

ARTICLE

pubs.acs.org/IC

Direct Evidence for Tautomerization of the Uracil Moiety within the Pb^{2+}/Uridine-5′-monophosphate Complex: A Combined Tandem Mass Spectrometry and IRMPD study

Jean-Yves Salpin,*[,†,‡] Sébastien Guillaumont,[†,‡] Daniel Ortiz,[†,‡] Jeanine Tortajada,[†,‡] and Philippe Maître*[,§,∥]

[†]Laboratoire Analyse et Modélisation pour la Biologie et l'Environnement and [‡]CNRS−UMR 8587, Université d'Evry Val d'Essonne, Bâtiment Maupertuis, Boulevard François Mitterrand, 91025 Evry, France

[§]Laboratoire de Chimie Physique and [∥]CNRS−UMR 8000, Université Paris Sud Orsay, Bâtiment 350, 91405 Orsay, France

Supporting Information

ABSTRACT: The structure of the $[Pb(UMP)-H]^+$ (UMP = uridine-5′-monophosphate) complex was studied in the gas phase by combining electrospray ionization (ESI), tandem mass spectrometry, and mid-infrared multiple photon dissociation (IRMPD) spectroscopy. The results obtained show that Pb^{2+} ions interact not only with the deprotonated phosphate group but also with a carbonyl group of the nucleobase moiety by folding of the mononucleotide, resulting in macrochelates that are not likely to be present in solution. Comparison between the IRMPD and DFT-computed spectra suggests that the ESI-generated complex likely corresponds to a mixture of several structures, and establishes the enolic tautomers as the most abundant species for the $[Pb(UMP)-H]^+$ ion, while the very weak IRMPD signal observed at ∼1763 cm^{-1} points to a minor population of oxo forms. Our data also suggest that losing the nucleobase residue under CID conditions does not necessarily mean a lack of interaction between the metal and the nucleobase moiety, as commonly reported in the literature for large oligonucleotides.

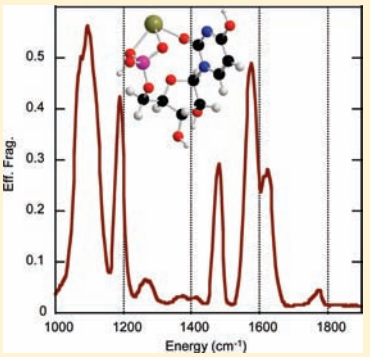

1. INTRODUCTION

Because of their polyanionic nature, the structure and biochemical functions of nucleic acids are clearly dependent upon their interactions with metal cations.[1−4] Metal ions may have antinomic effects on nucleic acids.[5] Magnesium and potassium cations, for example, play a crucial role in the stabilization of the secondary and tertiary structure of nucleic acids. Conversely, metals may also promote their loss of structure. This is the case of lead(II) ions which are particularly efficient in RNA depolymerization.[6] Pb^{2+}-induced hydrolysis of RNA has been widely studied,[7−9] and destabilization of DNA structure has also been reported.[10,11] Despite these known effects, the coordination chemistry between lead(II) ions and nucleic acid building blocks such as nucleotides, is hardly documented. Some years ago, Sigel and co-workers published several reports dealing with the interaction occurring in aqueous solution between Pb^{2+} ions and simple phosphates, phosphonates,[12] and nucleotides.[13,14] These potentiometric studies provided indirect information on the structure of both $[Pb(NMP)-2H]^\circ$ and $[Pb(NMP)-H]^+$ (NMP = nucleotide-5′-monophosphate) complexes.

While the interaction of metal complexes with nucleotides is one of the central topics in bioinorganic chemistry, studies about the gas-phase behavior of such interactions are scarce[15−29] compared to the numerous papers devoted to the interactions with peptides and proteins. A good knowledge of mechanisms at the molecular level is still lacking in most cases, and to the best of our knowledge, the gas-phase Pb^{2+}/nucleotides interactions have not been explored so far. In this context, we opted for a strategy based upon the gradual increase of the size of the nucleic acid building blocks, and began our studies with uracil[30] and thiouracils.[31] The present study reports the results obtained with one mononucleotide (Scheme 1), namely, uridine-5′-monophosphate (UMP).

As we shall see in details later (vide infra), electrospraying an aqueous mixture of lead nitrate and mononucleotides results in the formation in the gas phase of $[Pb(NMP)-H]^+$ ions, thereby allowing a direct comparison with data obtained in solution. To perform this study, we combined tandem mass spectrometry (MS/MS) experiments with theoretical density functional theory (DFT) calculations, and also recorded the IRMPD (Infrared Multiple Photon Dissociation) spectra of the electrospray ionization (ESI)-generated complexes. IRMPD spectroscopy of mass-selected ions is now established as a powerful approach for the structural characterization of gaseous ions and notably nucleotides,[32] and has been successfully applied to metal ion/biomolecules systems.[33−44] This ion spectroscopy is often termed "action spectroscopy" since IR absorption cannot be directly probed because of the low ion density within mass spectrometers. Nevertheless, through the use of intense infrared sources, ion fragmentation can be induced by a multiple photon absorption process. IRMPD spectra were presently recorded in the 1000−2000 cm^{-1} energy region by

Received: May 2, 2011
Published: July 11, 2011

Scheme 1

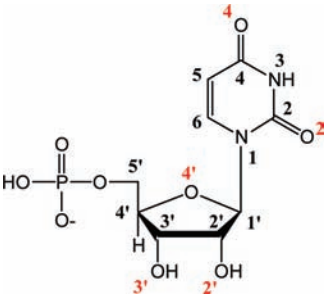

combining the CLIO (Centre Laser Infrarouge d'Orsay) free electron laser to a FT-ICR instrument.

2. EXPERIMENTAL AND THEORETICAL METHODS

2.1. Experimental Details. *Tandem Mass Spectrometry.* Electrospray mass spectra were recorded on a QSTAR PULSAR i (Applied Biosystems/MDS Sciex) hybrid instrument (QqTOF) fitted with an "ionspray" source. Lead nitrate/nucleotide mixtures at various concentrations were prepared either in pure water (purified with a Milli-Q water purification system) or in a water/methanol mixture (50/50 v/v), and were introduced in the source by infusion with a syringe pump at a flow rate of 4 μL/min. Ionization of the samples was achieved by applying a voltage of 5.0−5.4 kV on the sprayer probe and by the use of a nebulizing gas (GAS1, air) surrounding the sprayer probe. The operating pressure of GAS1 was adjusted to 1.4 bar by means of an electronic board (pressure sensors), as a fraction of the air inlet pressure. The curtain gas (N_2) was similarly adjusted to a value of 1.4 bar. To improve both ion transmission and sensitivity during the experiments, the collision gas (CAD, N_2) was present all along the ion path (up to the orthogonal injection chamber) for collisional focusing. The difference of potentials between the orifice plate and the skimmer (declustering potential, DP), typically referred to as the "cone voltage" for other electrospray interfaces, ranged from 20 to 80 V to perform the various experiments.

MS/MS spectra were systematically recorded at various collision energies ranging from 8 to 40 eV in the laboratory frame (the collision energy is given by the difference between the potentials of Q0 and Q2). The CAD parameter controlling the amount of N_2 introduced into Q2 was set to its minimum value to limit multiple ion−molecule collisions.

IRMPD Experiments. The present IRMPD study has been performed using an experimental platform based on FT-ICR into which pulsed IR light is coupled.[45] This particular experimental setup has already been described in detail elsewhere.[45] The most important feature for the present study is its quadrupole-hexapole interface between the electrospray source and the ICR cell. The bias voltage and RF amplitude of the quadrupole are adjusted to selectively transmit $[Pb(UMP)-H]^+$ complexes. Mass-selected ions are then trapped in a ∼5 cm long hexapole ion trap contained within a collision cell where ions normally are collisionally cooled using a flow of high-purity argon buffer gas. Ions are then pulse-extracted toward the ICR cell where mass-selection of the complexes is performed. They are then irradiated with IR light, after which the resulting fragment ions are mass-analyzed. $[Pb(UMP)-H]^+$ complexes were prepared in an ESI source by introducing Lead nitrate/UMP mixtures (10^{-4} M, water/methanol 50/50 v/v) in the source using direct infusion with a syringe pump. ESI conditions used are a flow rate of 3 μL/min, a spray voltage of 3500 V, and a capillary temperature of 200 °C.

IR spectroscopy was performed using the CLIO Free Electron Laser (FEL), which produces pulsed, tunable IR light covering the 100−2500 cm^{-1} wavenumber range.[46] The light is produced in an 8 μs long pulse train, the macropulse, of IR laser pulses a few picoseconds in duration, the micropulses. The macropulse repetition rate is 25 Hz while that of the micropulse is 62.5 MHz. In the present case, it can be noticed that only one or two trains of pulses were sufficient to achieve high photofragmentation yields (irradiation time 50−100 ms). Using an electron energy of 45 MeV, IRMPD spectra could be recorded over the 1000−2000 cm^{-1} energy range.

If the IR light is in resonance with an IR active vibrational mode of molecular ions stored in the ICR cell, IR photons can be absorbed by the ions and the sequential absorption of several IR photons can lead to fragmentation of the mass-selected ions. This photofragmentation, which is the result of a multiple photon absorption process, is often termed Infrared Multiple Photon Dissociation (IRMPD). By monitoring the number of detected ions in the parent mass channel and that in the fragment mass channels while varying the frequency of the IR light, an IR-MPD spectrum is obtained. For each wavelength, the mass spectrum is the Fourier transform of a time-domain transient averaged 5 times.

2.2. Theoretical Calculations. Molecular orbital calculations were carried out using the B3LYP[47,48] density functional, as implemented in the Gaussian-03 set of programs.[49] In a first step, the different structures were optimized with the dp-polarized 6-31G(d,p) basis, without any symmetry constraint. We used for Pb the "Stuttgart" quasi-relativistic pseudopotential developed by Küchle et al.[50] This particular 78 core−electrons effective core potential (ECP) employs a (4s,4p,1d)/[2s,2p,1d] basis set with a (3,1) contraction scheme for s and p functions that can be used directly in balance with the standard 6-31G(d,p) Pople basis set describing C, N, O, P, and H atoms. IR absorption spectra were computed at this level. Harmonic vibrational frequencies were also used to classify the stationary points as local minima or saddle points, and to estimate the zero-point vibrational energy (ZPE) corrections. Provided the use of an appropriate scaling factor, hybrid DFT methods such as B3LYP have been shown to outperform other DFT methods as well as traditional ab initio approaches to describe both position[51] and relative intensities[52] of IR bands. As far as the positions are concerned, a scaling factor value of 0.96 has been chosen on the basis of the overall good agreement between experimental and computed frequencies for a large set of molecules.[53]

To provide further insights about the interactions established between the metal and UMP, a natural population analysis (NPA) at the B3LYP/6-31G(d,p) level by means of the NBO program[54] has been carried out. Relative energies were refined using the 6-311+G(2df,2p) extended basis set. To this purpose, we developed for lead atom[55] a 6-311+G(2df) basis set, and demonstrated that this basis set, when combined with the B3LYP/Stuttgart approach, provide correct relative energies and constitute a good compromise between accuracy and computational cost.

Throughout this paper total energies are expressed in Hartree and relative energies in kJ/mol. For the sake of simplicity, the basis sets used for Pb will be referred to as 6-31G(d,p) and 6-311+G(2df,2p) basis sets. Detailed geometries (Cartesian coordinates) of all the structures mentioned in this paper are available from authors upon request.

3. RESULTS AND DISCUSSION

3.1. Mass Spectrometry. A typical positive-ion electrospray spectrum obtained when infusing a 1:1 aqueous mixture of lead nitrate and uridine-5′-monophosphate (10^{-4} M) using the QqTOF instrument is given in the Supporting Information, Figure S1. Lead-containing ions are easily identified because of the characteristic isotopic distribution of this element. The most prominent ion is always lead hydroxide $PbOH^+$ (m/z 225). At the pH of the aqueous mixtures (5.5), monucleotides are normally singly deprotonated and, expectedly, interaction with Pb(II) ions results in the formation of $[Pb(UMP)-H]^+$ complexes (m/z 531). Unlike what was

dx.doi.org/10.1021/ic200918q |*Inorg. Chem.* 2011, 50, 7769–7778

observed for nucleobases,[30,31] the abundance of the complex does not vary significantly with the declustering potential. Doubly charged complexes were not observed. Increasing the declustering potential induces the gradual disappearance of both lead hydroxide and the complex, and the appearance of bare Pb^+ ion. Some other lead-containing ions remain unassigned but probably arise from interaction with trace contaminants, such as the species detected at m/z 253, attributed to $Pb^{2+}/HCOO^-$ complex.

Other interesting species were also detected such as protonated uracil (m/z 113) and protonated uridine-5′-monophosphate (m/z 325).

A typical MS/MS spectrum obtained for the $[Pb(UMP)-H]^+$ complex (m/z 531) is given in Figure 1.

In-source fragmentation could also be performed by increasing the DP parameter, hence allowing to record MS/MS spectra for the most intense fragment ions. This set of experiments led to a dissociation pattern summarized in Scheme 2.

Starting from the precursor ion, two main processes are observed. The first one corresponds to the formation of protonated uracil, UH_2^+. Its intensity in the MS/MS spectra is very weak. Several studies dealing with the unimolecular reactivity of protonated[56−58] or lithium cationized[15] oligonucleotides showed that the abundance of BH_2^+ (B = nucleobase residue) ions was correlated with the relative gas-phase basicity of the nucleobases. The fact that formation of TH_2^+ ions was much less favored was indeed attributed to the lower gas-phase basicity of thymine compared to that of cytosine, adenine, or guanine.[59] Our MS/MS spectra support this finding.

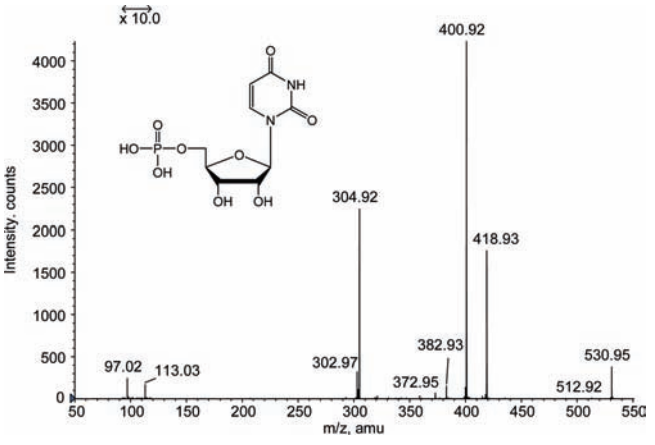

Figure 1. Low-energy MS/MS spectrum of the $[Pb(UMP)-H]^+$ (m/z 531) ion recorded at a collision energy of 22 eV (laboratory frame).

The second process originating from the precursor ion is the combined elimination of water and nucleobase (UH), leading to m/z 401 ions. This particular process has already been observed for Cat^+/TMP complexes (Cat = Li, Na, Cs).[15,21] A striking feature is that elimination of neutral uracil (UH) is particularly favorable, as attested by the abundant fragment ion detected at m/z 419 (Figure 1). Other ribo- and deoxyribo-mononucleotides have been investigated,[60] and it seems that elimination of neutral nucleobase is more pronounced in the case of ribo-mononucleotides, suggesting that the 2′ hydroxyl group might play an important role in this fragmentation process. Note that a very minor elimination of water is also observed (m/z 513).

Upon activation, m/z 401 ions give rise to m/z 97. This ion has been observed previously with protonated mono-[61] and dinucleotides.[56,57] Deuterium exchange experiments[56] have demonstrated that the m/z 97 ion exhibits one exchangeable proton. Consequently, this species is a sugar-derived ion (Scheme 2). Interestingly, the neutral fragment associated to the formation of this ion is $[PbHPO_4]$. Both this dissociation channel and the formation of the $[PbH_2PO_4]^+$ complex (m/z 305) would suggest that the metallic center should interact with the phosphate group. This is in agreement with the structures deduced from potentiometric studies by Sigel and co-workers.[12,14] However, the detection of the $[PbC_5H_3O_2]^+$ ion (m/z 303), which corresponds to the elimination of phosphoric acid from m/z 401, indicates that other coordination modes could be possible. Therefore, to complete our MS/MS data, quantum chemical calculations and IRMPD spectroscopy have been carried out.

3.2. Computational Results. A complete conformational analysis is already a challenging task for mononucleotides. Indeed, numerous geometrical parameters have to be taken into account: (i) the ring conformation, (ii) the hydroxymethyl and (iii) nucleobase orientation (*Syn* or *Anti*), (iv) the possibility of intramolecular hydrogen bonds (IMHBs), (v) the deprotonation site(s) of the nucleotide, and (vi) the site of coordination of the metal. However, previous results with pyrimidic nucleobases,[30,31] combined with the fact that the phosphate group is very likely deprotonated, allows us to restrict the number of possible initial geometries. Zwitterionic forms and π-coordination of the metal have been considered, and we also examined some structures in which the phosphate group is doubly deprotonated. In this last case, the nucleobase residue is protonated.

Representative structures obtained for $[Pb(UMP)-H]^+$ complexes, are presented in Figure 2, and relative energies of the various structures are summarized in the Supporting Information, Table S2. Relative energies were refined at the B3LYP/6-311+G(2df,2p) level, but this did not result in any significant

Scheme 2

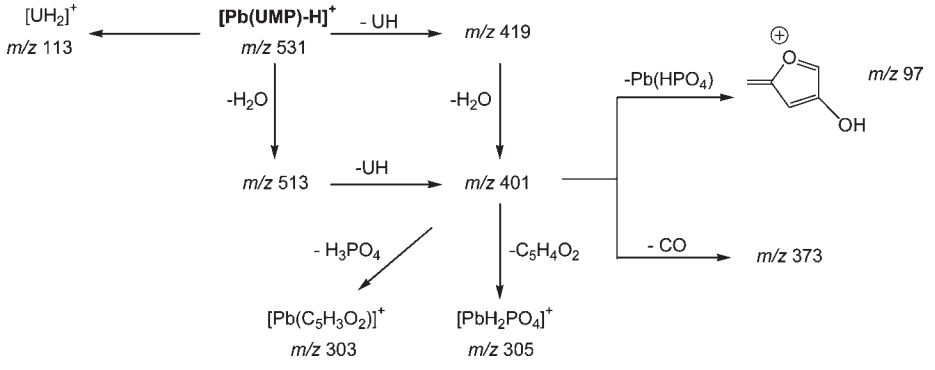

dx.doi.org/10.1021/ic200918q |*Inorg. Chem.* 2011, 50, 7769–7778

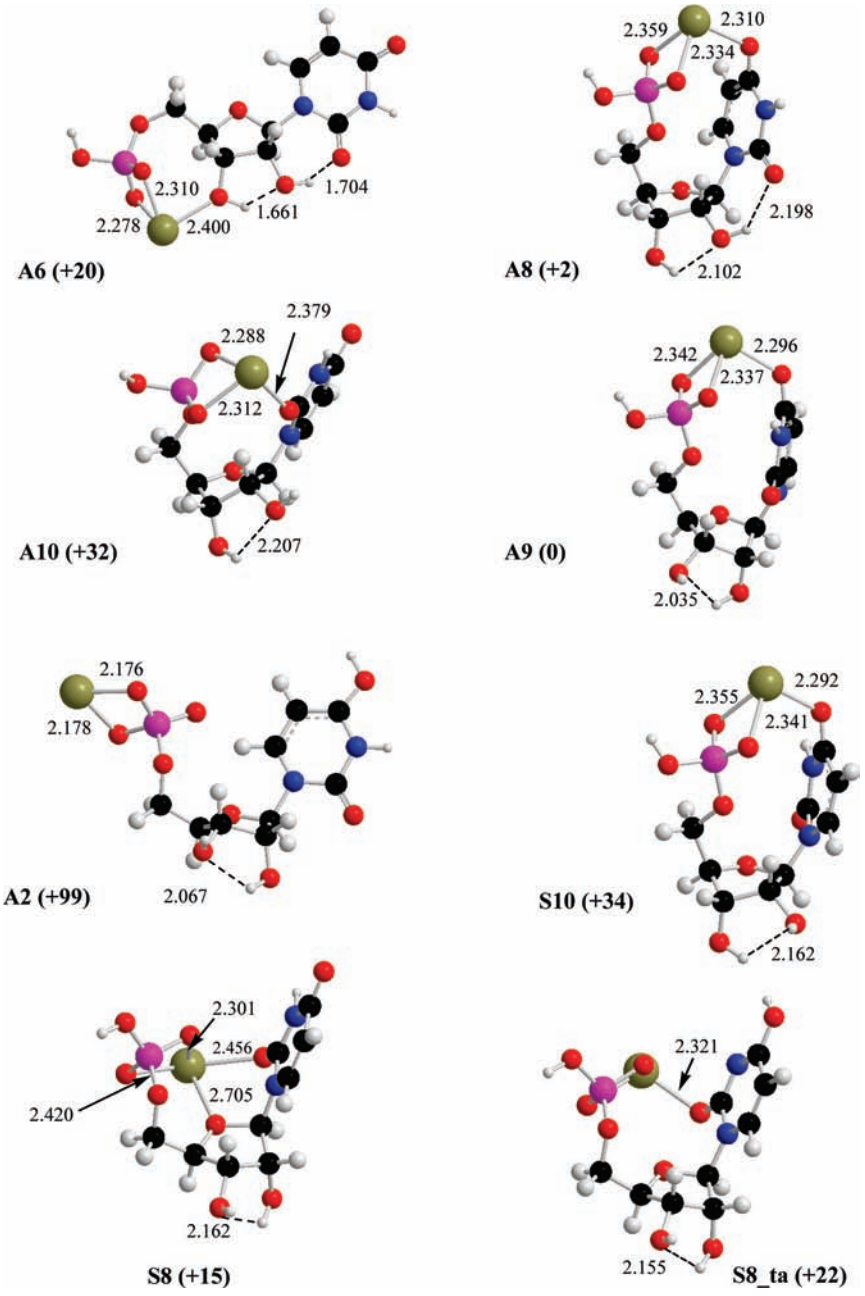

Figure 2. Relevant optimized structures of the $[Pb(UMP)\text{-}H]^+$ complex. Bond lengths are given in Angströms and relative energies in kJ mol^{-1}.

energy change. The various forms are labeled according to the *Syn* (S) or *Anti* (A) orientation of the nucleobase. The structure of all the forms investigated are provided in the Supporting Information.

Zwitterionic forms (**A11**−**13**), in which the phosphate group is singly deprotonated and the metallic center interacts with the base, appear to be local minima on the potential energy surface (no negative eigenvalues). However, these structures are predicted to be about 330−400 kJ/mol higher in energy than the global minimum (Supporting Information, Table S2) and therefore are not likely to be generated in the gas phase.

The **A6** form (Figure 2) is representative of the structure characterized in solution for the $[Pb(UMP)\text{-}H]^+$ complex. As a matter of fact, determination of stability constants associated with the formation of complexes between Pb^{2+} ions and phosphate monoesters or the mononucleotide[12,14] did not point out any Pb^{2+}/nucleobase interaction. **A6** appears particularly stable and is characterized by a bidentate interaction of the metal with two oxygen atoms of the phosphate group (Phos), and 2 IMHBs. This interaction mode is much more favorable than the situation in which one of the interacting oxygen atoms is replaced by the phosphate hydroxyl group (**A4**, +170 kJ/mol; Supporting Information, Figure S3). These results also indicate that like in solution,[14] the affinity of Pb^{2+} for the phosphate group is much stronger than the affinity for the nucleobase. However, **A6** does not correspond to the global minimum. Indeed, the five low-lying energy forms, which are all more stable than **A6**, share the same coordination scheme, with the metal interacting not only with

dx.doi.org/10.1021/ic200918q |*Inorg. Chem.* 2011, 50, 7769–7778

Table 1. Experimental and Computed Vibrational Bands for the $[Pb(UMP)-H]^+$ Complex

wavenumbers		DFT-computed intensities (km/mol)			
experimental	calculated	**A6**	**S8**	**S8_ta**	vibrational mode
1039−1145	1034			153	ν P−O
(1098)	1046		75		δ P−O−H
	1056	334	104		ν C4′−O4′
	1057			210	δ P−O−H
	1063	215			δ P−O−H
	1081			231	ν C2′−O2′
	1084	241			ν P−O5′
	1094			251	ν C2′−O2′
	1105	60			ν C2′−O2′
	1112		232		δ P−O−H
	1113	73			ν C4′−O4′
	1125		279		ν C5′−O5′
1189	1163			64	δ C2′−O2′−H
	1178			342	δ C4−O4−H tautom.
	1179		33		δ C−C−H
	1181		24		δ C′−C′−H
	1183	50			δ C−C−H +δ C′−C′−H
	1186		75		δ C3′−O3′−H
	1187			30	δ C′−O′−H +δ C′−C′−H
1271	1255	171			δ C′−C′−H
1476	1468			504	ν C4═O4
1576	1539			90	ν C4═C5 + ν C2═O2 s
	1555			514	ν C4═C5 + ν C2═O2 as
1621	1603		414		ν C2═O2
	1618	67			ν C5═C6
	1623			562	ν C5═C6
	1642		547		ν C5═C6
	1691	592			ν C2═O2
1763	1764	530			ν C4═O4
	1767				ν C2═O2
	1777		500		ν C4═O4

the phosphate moiety but also with one of the carbonyl group of the nucleobase. This result is not surprising as our previous studies on uracil[30] and thiouracils[31] already demonstrated the strong affinity of lead(II) ions toward carbonyl groups. The most stable structure obtained during the DFT study (**A9**, Figure 2) is characterized by a tridentate coordination involving the phosphate and the C4═O4 carbonyl group of an *Anti*-oriented uracil. A strong interaction with the carbonyl group is established as attested by the important bond lengthening (1.277 Å while the C2═O2 bond length is only 1.211 Å) and induces a significant distortion of the pyrimidic ring. Similar forms have been already described as particularly stable by Mazzuca et al. for the Al^{3+}/UMP complex.[62] Interaction with Pb^{2+} in the gas phase therefore promotes the folding of the mononucleotide to maximize the number of interactions. The sugar-ring conformation does not seem to have a strong influence on this particular coordination scheme, as attested by the very small energy difference (2 kJ/mol) between **A9** ($^3T_2$) and **A8** ($^4T_3$). This is the other way around when considering the nucleobase orientation, as the *Syn* form **S10** (+34 kJ/mol, Figure 2) is significantly less stable than **A8** (+2 kJ/mol).

Interaction with both the phosphate and the C2═O2 carbonyl groups has also been envisaged. The most stable forms are obtained when the nucleobase adopts a *Syn* orientation (**S7** and **S8**). Examination of Table 1 indicates that, like for D-glucose,[63] an additional interaction with the endocyclic O4′ oxygen atom provides an extra stabilization, since both **S7** and **S8** are 17 and 19 kJ/mol more stable than **S9**, respectively. It is worth noting that the **A9** and **S8** structures are practically degenerate when performing MP2 calculations (Supporting Information, Table S2), and **S8** becomes the global minimum at the MP2/6-311+G(2df,2p)//MP2/6-31G(d,p) level.

We failed in optimizing a complex in which the metal was π-coordinated to the pyrimidic ring (apical form), all the structures evolving toward an association with one of the carbonyl groups. Interestingly, one of our attempts (**A1**, Supporting Information, Figure S3) led to an interaction between the metal and the carbon C5, which rehybridizes from sp^2 to sp^3.

As mentioned previously, structures with a doubly deprotonated phosphate group were also considered because the elimination of $[PbHPO_4]$ was detected in weak abundance during MS/MS experiments. These forms (**A2**, **A3**, **S2**, and **S3**) do

dx.doi.org/10.1021/ic200918q |*Inorg. Chem.* 2011, 50, 7769–7778

correspond to local minima but are high in energy (about 100−153 kJ/mol above **A9**). Note that these forms are more stable when the nucleobase adopts an *Anti* orientation.

The natural population analysis (NPA) shows a transfer of electrons to the lead atom, the local charge on Pb ranging from 1.16 for the zwitterionic forms up to 1.53 for the macrochelates. The fact that the charge transfer is more pronounced for zwitterions is not surprising because it has been shown that the amount of electron transfer increases as the electronegativity of the ligand decreases.[64] Natural electron configuration analysis indicates that the electron transfer is mostly in the 6p orbitals of the metal (typical electron configuration being: 6s[1.93] 6p[0.53]$sp^{0.27}$). The Pb(II) lone pair is predominantly 6s, but is slightly polarized by a small 6p contribution. This feature is characteristic of the ionic character of the bonds.[64] The 6p contribution ranges from 1.5% for zwitterions up to 5.2% for macrochelates. More electron density is indeed transferred to the lead atom when the ligands carry a formal negative charge, such as the phosphate group.

To summarize, gas-phase interactions of Pb^{2+} ions with UMP differ from those of alkali metals and Cu^{+} ions. Whereas the latter tend to bind exclusively the phosphate group,[15,17,18,21,65] the former promote the folding of the mononucleotide, and lead to macrochelates in which the metal ion is coordinated between the phosphate oxygens and the nucleobase. Such a binding mode has already been proposed for Cr(III)/dinucleotides[16] and Fe(III)/trinucleotides[65] systems. However, the interaction with the nucleobase cannot be directly deduced from MS/MS experiments, since the loss of the nucleobase is very facile and the Pb/nucleobase complex is not detected (Figure 1). Finally, as at least six different structures lie within a 20 kJ/mol energy range for both systems, the complexes produced in the gas phase by ESI might correspond to a mixture of different species. Thus, IRMPD spectroscopy experiments have been performed to get more insight. Results are presented in the next section.

3.3. IRMPD Spectroscopy. IRMPD spectroscopy has been widely applied to characterize the structure of metal-cationized complexes,[66] but most of the studies dealt with interactions involving aminoacids and peptides. One may cite, however, several IRMPD studies of Fridgen and co-workers dealing with the interaction of Li^{+} with nucleobases,[39,43,44] carried out in the N−H and O−H stretching region (2600−3900 cm^{-1}). Presently, IRMPD spectra have been recorded in the 1000−2000 cm^{-1} energy range. On resonance with an infrared active mode of the mass-selected ions, the elimination of uracil with or without water is observed, consistent with CID results. It should be pointed out that the two corresponding mass-resolved IR photofragmentation spectra are similar. The maximum fragmentation yield was about 20% using only a single IR-FEL macropulse, suggesting an excellent spatial overlap between the laser and the ion cloud and/or low threshold dissociation energies.[67] In the following, IRMPD spectra correspond to the fragmentation efficiency, defined as −ln[Precursor/(Precursor + Fragments)], as a function of the photon wavenumber.[68] A recent study[69] has demonstrated that this data treatment allows a better comparison with calculated infrared absorption spectra and a better spectral resolution than other analysis methods such as recording a depletion spectrum or calculating a photodissociation yield.

The IRMPD spectrum obtained for the $[Pb(UMP)\text{-}H]]^{+}$ complex is given in Figure 3a. To facilitate the assignment of the various IR bands associated with the phosphate group, the IR photodissociation spectrum of the $[Pb(H_2PO_4)]^{+}$ ion (m/z 305) has also been recorded between 800 and 1600 cm^{-1} (Figure 3b). Finally the IRMPD spectrum of the $[Pb(uridine)\text{-}H]^{+}$ ion generated

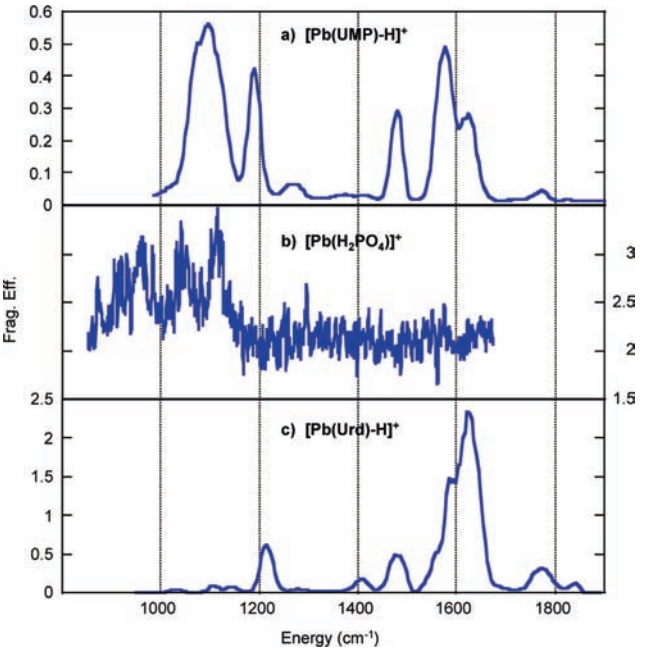

Figure 3. Experimental IRMPD spectra obtained for (a) the $[Pb(UMP)\text{-}H]^{+}$, (b) $[Pb(H_2PO_4)]^{+}$, and (c) $[Pb(uridine)\text{-}H]^{+}$ complexes. See text for details.

with the nucleoside uridine, which does not contain any phosphate group, is also reported in Figure 3c. A detailed interpretation of the two latter spectra is clearly beyond the scope of the present study, but the comparison between the three spectra gives useful insights for the assignment of the experimental bands of Figure 3a. Examination of Figure 3 indeed clearly indicates that some of the experimental features observed between 800 and 1150 cm^{-1} are characteristic of the cationized phosphate group. As a matter of fact, no noticeable photofragmentation is detected above 1150 cm^{-1} for the Pb^{2+}/phosphate system (Figure 3b), whereas no signal is detected under 1100 cm^{-1} for the $[Pb(uridine)\text{-}H]^{+}$ complex. Therefore, the very broad feature (fwhm = 100 cm^{-1}) centered at 1100 cm^{-1} on Figure 3a may corresponds to active modes of the cationized phosphate group. It is also worth noting that all the other intense features detected in Figure 3a above 1150 cm^{-1} do not involve the phosphate group. Note also that the IRMPD spectrum of the free deprotonated phosphate group $H_2PO_4^{-}$ has been recently recorded,[70] and a band attributed to the asymmetric PO_2^{-} stretching mode was detected at 1297 cm^{-1}. As no noticeable signals are detected above 1150 cm^{-1} in Figure 3b, this vibrational mode is red-shifted because of the interaction with the metal.

Detailed assignment of the IRMPD spectrum is based on its comparison with the spectra computed for various low-energy lying isomers, whose vibrational bands are summarized in Table 1. In making these comparisons, one should keep in mind that the calculated IR intensities often do not correspond well with the multiple photon spectrum, because of the complex nature of the IRMPD process.[68,71,72] To make the comparison easier, computed absorption cross sections are represented in Figure 4 by assuming a Gaussian profile (fwhm = 15 cm^{-1}) for each calculated infrared band.

As mentioned previously, the IRMPD spectrum of the $[Pb(UMP)\text{-}H]^{+}$ complex (Figure 3a,4a) is dominated by a very broad band (fwhm = 100 cm^{-1}) centered at 1100 cm^{-1}, displaying a symmetric profile. When the same experimental setup is used, isolated IR-active vibrational modes give rise to narrower

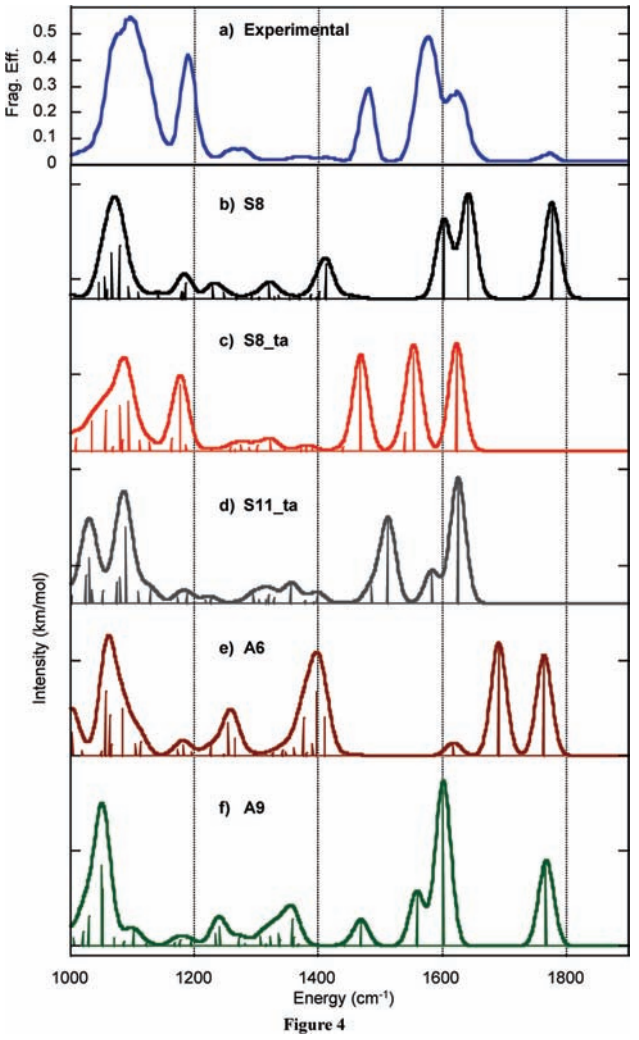

Figure 4. IRMPD spectrum (a) obtained for the $[Pb(UMP)-H]^+$ complex compared to DFT-computed IR absorption spectra (b−f) of some relevant structures. See text for details.

IRMPD bands with a width of 15−20 cm^{-1}.[45] Consequently, this broad feature is very likely the result of the superposition of two or more features, which result from multiple photon absorption through different active IR modes. This is consistent with the data both deduced from Figure 3 and given in Table 1, which show that numerous vibrational modes (and notably P−O and C′−O′ stretches, P−O−H bending mode) are computed in this energy range. Expectedly, because of the interaction with the metal, the P−O stretch is strongly red-shifted as compared to that observed for uncomplexed phosphate groups.[70]

Two other intense but narrower symmetric bands are detected at about 1189 and 1476 cm^{-1}. A large asymmetric feature is also observed and corresponds to two bands at 1576 and 1631 cm^{-1}. Finally, three weak signals could be detected at about 1271, 1400, and 1763 cm^{-1}.

The C═O stretching mode constitutes an excellent infrared diagnostic of the presence of the bare oxo forms, especially in the case of the uracil moiety which includes two carbonyl groups. The DFT-calculated IR absorption spectrum of the solution-like structure (**A6**) is given in Figure 4e. The calculated frequencies for the two C═O stretches are 1764 and 1691 cm^{-1}. The former corresponds to the "free" C4═O4 carbonyl group. The C2═O2 carbonyl group is involved in a strong IMHB with the O2′H hydroxyl group, which results in a slight bond lengthening/weakening (1.238 Å compared to 1.212 Å for C4═O4) and therefore in a red-shift of the computed frequency. The weak band observed experimentally at 1763 cm^{-1} might correspond to the C4═O4 stretch. However, there is no strong experimental signal around 1400 and 1700 cm^{-1}. In addition, the computed spectrum of **A6** cannot account for the intense band detected at 1189 cm^{-1}. Given this strong discrepancy, the formation in the gas phase of solution-like structures can be ruled out.

The computed IR spectrum of representative *Anti* (**A9**) and *Syn* (**S8**) macrochelates are reported in Figure 4f and 4b, respectively. DFT spectra show that many IR active modes lie in the 1000−1100 cm^{-1} energy range, in agreement with the very broad band observed experimentally. Similarly, the weak experimental features detected between 1250 and 1400 cm^{-1} could be attributed to combined C−C−H and C′−O′−H bending modes. Both **A9** and **S8** are characterized by one "free" carbonyl group and one carbonyl group interacting with the metallic center. The "free" C═O stretches are computed at 1767 and 1777 cm^{-1}, for **A9** and **S8**, respectively. These values are in good agreement with the weak feature observed at 1763 cm^{-1}. Interaction of Pb^{2+} ion with the second carbonyl group is characterized by a very strong bond activation, as attested by the computed C═O bond lengths (C4═O4 = 1.277 Å and C2═O2 = 1.256 Å, for **A9** and **S8**, respectively). Accordingly, the IR stretching mode for these two bonds is significantly red-shifted, and lies at 1559 and 1603 cm^{-1}, respectively. These red-shifts (>150 cm^{-1}) are much stronger than those induced by alkali metal cations[73] (41−61 cm^{-1}) or Ba^{2+}[38](∼100 cm^{-1}) when interacting with aminoacids, thus underlying the particularly strong affinity of Pb^{2+} ions toward carbonyls.

For both **A9** and **S8**, the most active vibrational mode corresponds to the C5═C6 double bond stretch and is located around 1600 cm^{-1}. In fact, the presence of two strongly active IR modes in the 1550−1650 cm^{-1} energy range is a general trend for the most stable macrochelate forms and may account for the asymmetric feature observed experimentally in the 1550−1650 cm^{-1} energy range. Note that given the very small energy gap between *Syn* and *Anti* structures, a mixture of both *Syn* and *Anti* macrochelates might be generated in the gas phase. This assumption is supported by the fact that **S8** and **A9** are practically degenerate according to our MP2 calculations (see Supporting Information, Table S2), and that the activation barrier associated with the *Syn/Anti* interconversion in solution is particularly weak (estimated at 6−8 kJ/mol for cytidine-monophosphate[74]). Such mixtures would even better reproduce the experimental trace observed between 1530 and 1650 cm^{-1}.

The IRMPD signal observed at 1763 cm^{-1} supports the presence of one or several macrochelate oxo forms in the gas phase. However, examination of Figure 4 shows that oxo forms cannot account for the two strong experimental bands observed at 1189 and 1476 cm^{-1}. Furthermore, the computed infrared cross-section associated with the free carbonyl group is systematically strong; it is therefore somewhat surprising to observe a relatively small fragmentation efficiency in resonance with this vibrational mode. We already observed such a weak IRMPD signal at these particular wavelengths for protonated uracil, and our IRMPD experiments, performed either in the 1000−2000 cm^{-1} range[75] or in the in the NH and OH stretching region,[76] demonstrated that for protonated uracil enolic tautomers were predominantly generated in the gas phase. Thus, starting from the most stable

dx.doi.org/10.1021/ic200918q |*Inorg. Chem.* 2011, 50, 7769–7778

oxo forms, we also considered a series of enolic tautomers, by moving the proton of N3 onto the adjacent free carbonyl group.

Examination of Supporting Information (Table S2) indicates that tautomeric forms lie only several kJ/mol above their oxo counterpart, and that some are particularly stable. The most stable one, **S8_ta**, shares the same coordination scheme as **S8**, and formally arises from the latter through a 1,3 hydrogen shift between the N3 and O4 atoms. Its DFT-calculated IR absorption spectrum is given in Figure 4c. It strikingly reproduces both the positions and relative intensities of the experimental bands, and notably those at 1476 and 1189 cm^{-1}, which can be assigned to ν_{C4O4} and $\delta_{C4-O4-H}$ bending mode (newly formed hydroxyl group), respectively (Table 1). These two bands therefore strongly suggest the presence of enolic complexes in the gas phase.

Finally, Figure 4d displays the computed IR spectra of the enolic tautomer **S11_ta**. This form in fact is the tautomer of **A9**, but isomerization is accompanied with a slight rotation of the uracil residue, which then adopts a *Syn* orientation. The IR enolic signatures (ν_{C2O2} and $\delta_{C2-O2-H}$) are computed at 1486 and 1513 cm^{-1}, whereas the experimental IRMPD signal vanishes around 1510 cm^{-1}. As a similar observation can be made for the band computed at 1030 cm^{-1}, formation of **S11_ta** thus seems unlikely.

4. DISCUSSION

The IRMPD study indicates that a mixture of both oxo and enolic macrochelates, such as **S8** and **S8_ta** structures, is generated in the gas phase for the $[Pb(UMP)\text{-}H]^+$ complex, suggesting tautomerization of the UMP moiety in solution or within the electrospray droplets. On the other hand, solution-like structures such as **A6** are not formed.

Even if rigorous quantitation cannot be made, the disagreement between experimental and computed intensities for the free C═O stretch indeed establishes the enolic tautomers as the prominent species for the $[Pb(UMP)\text{-}H]^+$ complex under our experimental conditions. Consequently, tautomerization of either neutral or complexed uracil moiety must be envisaged to account for the formation of enolic tautomers. This isomerization process may occur prior to the interaction with the metal cation, but only with the requirement that the uncomplexed system is already solvated by water.

We have shown in a previous study[75] that tautomerization of the isolated neutral uracil is energy-demanding and can be reasonably ruled out. For example, the activation barrier associated with the 1,3H-shift between N3(H) and O4 was located 168.4 kJ/mol above the dioxo form. On the other hand, this process is significantly facilitated by protic solvent molecule(s). The most stable structure of uracil-water cluster corresponds to a structure where the water molecule forms a bridge between O4 and N3(H) of canonical uracil.[75,77,78] This configuration is favorable for a potential water-catalyzed double proton transfer. The corresponding transition state is hexahedric, water acting as a bridge. We observed (see the Supporting Information of ref 75) that the formation of this six-membered ring considerably lowers the activation energy (estimated at 67.1 kJ.mol^{-1}). Furthermore, Hu et al. have shown that adding a second molecule of water in the N3−O4 region further decreases the activation barrier for tautomerization.[78]

Alternatively, tautomerization could also occur after the complexation by the metal. Our previous study[30] indeed pointed out that Pb^{2+}-cationization induces the stabilization of the enolic uracil moiety, provided the metal is coordinated to a carbonyl group. This is illustrated by the Supporting Information (Figure S2) which shows that the enolic form is located about 30 kJ/mol above the dioxo complex, while for neutral uracil this energy gap was estimated to 48 kJ/mol.[75] Furthermore, Pb^{2+}-complexation also lowers the activation barrier associated to the 1,3H-shift between N3 and O4 (+152 kJ/mol). However, this barrier remains very important, and such a process is precluded in the gas phase at thermal energy. On the other hand, in presence of solvent, the stabilization is strongly enhanced as demonstrated by Figure S2 (Supporting Information). Upon addition of one water molecule, the activation barrier associated to the proton transfer is further lowered and now lies 41 kJ/mol above the dioxo form, and the two tautomers are now nearly degenerate. The potential energy surface associated with the **S8→S8_ta** interconversion through a water catalyzed double proton transfer has also been explored and similar energies are obtained (Supporting Information, Figure S2). The energy gap between both forms is slightly reduced, and the activation barrier is located 40 kJ/mol above **S8_ta.** Consequently, it is conceivable that water-assisted tautomerization of UMP in solution or within the electrospray droplets, prior to or after the complexation process, may lead to the enolic forms evidenced by IRMPD, and that the metal may further facilitate this isomerization (catalytic role).

5. CONCLUSION

The present study unambiguously demonstrates that the structure of the $[Pb(UMP)\text{-}H]^+$ complex in the gas phase differs from that postulated in solution from potentiometric studies. While MS/MS spectra indicate that the metal indeed interacts with the phosphate group, mid-infrared multiple photon dissociation spectroscopy clearly shows that Pb^{2+} ions also promote the folding of the mononucleotide and strongly interacts with one of the carbonyl groups of the nucleobase moiety. It is worth mentioning that this particular interaction does not prevent the complexes from expelling the nucleobase under CID conditions. Consequently, losing the nucleobase does not necessarily mean a lack of interaction between the metal and the nucleobase moiety, as commonly mentioned for large oligonucleotides. Additional experiments are on the way to check if a similar behavior is observed with bigger oligonucleotides.

IRMPD experiments show that the ESI-generated complexes probably correspond to a mixture of keto and enolic forms, and establish the latter ones as the most abundant species for the $[Pb(UMP)\text{-}H]^+$ complex. It is proposed that tautomerization of either neutral or complexed UMP should be relatively facile in a protic solvent, prior to or during their transfer into the gas phase by the electrospray process, and that tautomerization is further facilitated by Pb^{2+} complexation. Therefore, this metal dication, by catalyzing the enolization process, might favor base mispairing which is one of the origins of gene mutation.[79,80]

■ ASSOCIATED CONTENT

Supporting Information. Further details are given in Figures S1−S4 and Tables S1−S2. This material is available free of charge via the Internet at http://pubs.acs.org.

■ AUTHOR INFORMATION

Corresponding Author

*Phone: 33 1 69 47 76 44 (J.-Y.S.). Fax: 33 1 69 47 76 55 (J.-Y.S.). E-mail: jean-yves.salpin@univ-evry.fr (J.-Y.S.).

■ ACKNOWLEDGMENT

The authors gratefully acknowledge the European Commission for a generous grant (EC15637, sixth FP). They thank the CLIO team (J. M. Ortega, C. Six, G. Perilhous, J. P. Berthet) for their support during the experiments. Financial support from CNRS (Centre National de la Recherche Scientifique) through the TGE high-resolution FT-ICR for conducting the research is gratefully acknowledged.

■ REFERENCES

(1) *Interactions of Metal Ions with Nucleotides: Nucleic Acids, and Their Constituents*; Marcel Dekker: New York, 1996; Vol. 33.
(2) Burrows, C. J.; Muller, J. G. *Chem. Rev.* **1998**, *98*, 1109–1151.
(3) Harford, C.; Sarkar, B. *Acc. Chem. Res.* **1997**, *30*, 123–130.
(4) Lippert, B. *Coord. Chem. Rev.* **2000**, *200*, 487–516.
(5) Saenger, W. *Principles of nucleic acid structure*; Springer-Verlag: New York, 1984; p 556.
(6) Farkas, W. R. *Biochim. Biophys. Acta* **1968**, *155*, 401–409.
(7) Brown, R. S.; Hingerty, B. E.; Dewan, J. C.; Klug, A. *Nature* **1983**, *303*, 543–546.
(8) Brown, R. S.; Dewan, J. C.; Klug, A. *Bochemistry* **1985**, *24*, 4785–4801.
(9) Scott, W. G. *Curr. Opin. Chem. Biol.* **1999**, *3*, 705–709.
(10) Swiatek, J.; Gulanowski, B. *Acta Biochim. Pol.* **1990**, *37*, 7–20.
(11) Smirnov, I.; Shafer, R. H. *J. Mol. Biol.* **2000**, *296*, 1–5.
(12) Da Costa, C. P.; Sigel, H. *J. Biol. Inorg. Chem.* **1999**, *4*, 508–514.
(13) Da Costa, C. P.; Sigel, H. *Inorg. Chem.* **2000**, *39*, 5985–5993.
(14) Sigel, H.; Da Costa, C. P.; Martin, R. B. *Coord. Chem. Rev.* **2001**, *219*, 435–461.
(15) Rodgers, M. T.; Campbell, S. A.; Beauchamp, J. L. *Int. J. Mass Spectrom. Ion Processes* **1997**, *161*, 193–216.
(16) Madhusudanan, K. P.; Katti, S. B.; Vijayalakshmi, R.; Nair, B. U. *J. Mass Spectrom.* **1999**, *34*, 880–884.
(17) Favre, A.; Gonnet, F.; Tabet, J. C. *Int. J. Mass Spectrom.* **1999**, *191*, 303–312.
(18) Wang, Y.; Taylor, J. S.; Gross, M. L. *J. Am. Soc. Mass Spectrom.* **2001**, *12*, 550–556.
(19) Wang, Y.; Taylor, J. S.; Gross, M. L. *J. Am. Soc. Mass Spectrom.* **2001**, *12*, 1174–1179.
(20) Beck, J. L.; Colgrave, M. L.; Ralph, S. F.; Sheil, M. M. *Mass Spectrom. Rev.* **2001**, *20*, 61–87.
(21) Xiang, Y.; Abliz, Z.; Takayama, M. *J. Am. Soc. Mass Spectrom.* **2004**, *15*, 689.
(22) Keller, K. M.; Brodbelt, J. S. *J. Am. Soc. Mass Spectrom.* **2005**, *16*, 28–37.
(23) Monn, S. T. M.; Schurch, S. *J. Am. Soc. Mass Spectrom.* **2005**, *16*, 370–378.
(24) Cheng, P.; Bohme, D. K. *J. Phys. Chem. B* **2007**, *111*, 11075–11082.
(25) Barlow, C. K.; Hodges, B. D. M.; Xia, Y.; O'Hair, R. A. J.; McLuckey, S. A. *J. Am. Soc. Mass Spectrom.* **2008**, *19*, 281–293.
(26) Egger, A. E.; Hartinger, C. G.; Hamidane, H. B.; Tsybin, Y. O.; Keppler, B. K.; Dyson, P. J. *Inorg. Chem.* **2008**, *47*, 10626–10633.
(27) Anichina, J.; Bohme, D. K. *J. Phys. Chem. B* **2009**, *113*, 328–335.
(28) Flosadottir, H. D.; Stano, M.; Ingolfsson, O. *J. Am. Soc. Mass Spectrom.* **2009**, *20*, 689–696.
(29) Anichina, J.; Bohme, D. K. *Influence of metal ions on the structure and reactivity of nucleic acids*; CRC Press: Boca Raton, FL, 2010.
(30) Guillaumont, S.; Tortajada, J.; Salpin, J. Y.; Lamsabhi, A. M. *Int. J. Mass Spectrom.* **2005**, *243*, 279–293.
(31) Salpin, J. Y.; Guillaumont, S.; Tortajada, J.; Lamsabhi, A. M. *J. Am. Soc. Mass Spectrom.* **2009**, *20*, 359–369.
(32) Chiavarino, B.; Crestoni, M. E.; Fornarini, S.; Lanucara, F.; Lemaire, J.; Maitre, P.; Scuderi, D. *Int. J. Mass Spectrom.* **2008**, *270*, 111–117.
(33) Kapota, C.; Lemaire, J.; Maitre, P.; Ohanessian, G. *J. Am. Chem. Soc.* **2004**, *126*, 1836–1842.
(34) Polfer, N. C.; Oomens, J.; Dunbar, R. C. *Phys. Chem. Chem. Phys.* **2006**, *8*, 2744–2751.
(35) Dunbar, R. C.; Polfer, N. C.; Oomens, J. *J. Am. Chem. Soc.* **2007**, *129*, 14562–14563.
(36) Polfer, N. C.; Oomens, J.; Dunbar, R. C. *ChemPhysChem* **2008**, *9*, 579–589.
(37) Balaj, O. P.; Kapota, C.; Lemaire, J.; Ohanessian, G. *Int. J. Mass Spectrom.* **2008**, *269*, 196–209.
(38) Bush, M. F.; Oomens, J.; Saykally, R. J.; Williams, E. R. *J. Am. Chem. Soc.* **2008**, *130*, 6463–6471.
(39) Gillis, E. A. L.; Rajabi, K.; Fridgen, T. D. *J. Phys. Chem. A* **2009**, *113*, 824–832.
(40) Brodbelt, J. S.; Wilson, J. J. *Mass Spectrom. Rev.* **2009**, *28*, 390–424.
(41) Eyler, J. R. *Mass Spectrom. Rev.* **2009**, *28*, 448–467.
(42) Polfer, N. C.; Oomens, J. *Mass Spectrom. Rev.* **2009**, *28*, 468–494.
(43) Gillis, E. A. L.; Fridgen, T. D. *Int. J. Mass Spectrom.* **2010**, *297*, 2–8.
(44) Rajabi, K.; Gillis, E. A. L.; Fridgen, T. D. *J. Phys. Chem. A* **2010**, *114*, 3449–3456.
(45) Bakker, J. M.; Besson, T.; Lemaire, J.; Scuderi, D.; Maitre, P. *J. Phys. Chem. A* **2007**, *111*, 13415–13424.
(46) Prazeres, R.; Glotin, F.; Insa, C.; Jaroszynski, D. A.; Ortega, J. M. *Eur. Phys. J. D* **1998**, *3*, 87–93.
(47) Lee, C.; Yang, W.; Parr, R. G. *Phys. Rev. B* **1988**, *37*, 785–789.
(48) Becke, A. D. *J. Chem. Phys.* **1993**, *98*, 5648–5652.
(49) Frisch, M. J.; Trucks, G. W.; Schlegel, H. B.; Scuseria, G. E.; Robb, M. A.; Cheeseman, J. R.; Zakrzewski, V. G.; J.A. Montgomery, J.; Vreven, T.; Kudin, K. N.; Burant, J. C.; Millam, J. M.; Iyengar, S. S.; Tomasi, J.; Barone, V.; Mennucci, B.; Cossi, M.; Scalmi, G.; Rega, N.; Petersson, G. A.; Nakatsuji, H.; Hada, M.; Ehara, M.; Toyota, K.; Fukuda, R.; Hasegawa, J.; Ishida, M.; Nakajima, T.; Honda, Y.; Kitao, O.; Adamo, C.; Jaramillo, J.; Gomperts, R.; Stratmann, R. E.; Yazyev, O.; Austin, J.; Cammi, R.; Pomelli, C.; Ochterski, J.; Ayala, P. Y.; Morokuma, K.; Voth, G. A.; Salvador, P.; Dannenberg, J. J.; Zakrzewski, V. G.; Dapprich, S.; Daniels, A. D.; Strain, M. C.; Farkas, O.; Malick, D. K.; Rabuck, A. D.; Raghavachari, K.; Foresman, J. B.; Ortiz, J. V.; Cui, Q.; Baboul, A. G.; Clifford, S.; Cioslowski, J.; Stefanov, B. B.; Liu, G.; Liashenko, A.; Piskorz, P.; Komaromi, I.; Martin, R. L.; Fox, D. J.; Keith, T.; Al-Laham, M. A.; Peng, C. Y.; Nanayakkara, A.; Challacombe, M.; Gill, P. M. W.; Johnson, B.; Chen, W.; Wong, M. W.; Gonzalez, C.; Pople, J. A. *Gaussian03*, Revision C.02; Gaussian, Inc.: Wallingford, CT, 2003.
(50) Küchle, W.; Dolg, M.; Stoll, H.; Preuss, H. *Mol. Phys.* **1991**, *6*, 1945–1963.
(51) Halls, M. D.; Velkovski, J.; Schlegel, H. B. *Theor. Chem. Acc.* **2001**, *105*, 413–421.
(52) Halls, M. D.; Schlegel, H. B. *J. Chem. Phys.* **1998**, *109*, 10587–10593.
(53) Johnson, R. D., III *NIST Computational Chemistry Comparison and Benchmark Database. NIST Standard Reference Database Number 101*; National Institute of Standards and Technology: Gaithersburg, MD, 2005.
(54) Glendening, E. D.; Reed, A. E.; Weinhold, F. *NBO*, version 3.1.
(55) Salpin, J. Y.; Tortajada, J.; Alcamí, M.; Mó, O.; Yáñez, M. *Chem. Phys. Lett.* **2004**, *383*, 561–565.
(56) Phillips, D. R.; McCloskey, J. A. *Int. J. Mass Spectrom. Ion Processes* **1993**, *128*, 61–82.
(57) Rodgers, M. T.; Campbell, S.; Marzluff, E. M.; Beauchamp, J. L. *Int. J. Mass Spectrom. Ion Processes* **1995**, *148*, 1–23.
(58) Ni, J.; Mathews, M. A. A.; McCloskey, J. A. *Rapid Commun. Mass Spectrom.* **1997**, *11*, 535–540.
(59) Lias, S. G.; Bartmess, J. E.; Liebman, J. F.; Holmes, J. L.; Levin, R. D.; Mallard, W. G. *Ion Energetics Data*; National Institute of Standards and Technology: Gaithersburg, MD.
(60) Salpin, J.-Y.; Gamiette, L.; Tortajada, J.; Besson, T.; Nicol, E.; Maitre, P. *Int. J. Mass Spectrom.* **2011**, *304*, 154−164
(61) Sakurai, T.; Matsuo, T.; Kusai, A.; Nojima, K. *Mass Spectrom.* **1989**, *3*, 212–216.

(62) Mazzuca, D.; Russo, N.; Toscano, M.; Grand, A. *J. Phys. Chem. B* **2006**, *110*, 8815–8824.
(63) Salpin, J. Y.; Tortajada, J. *J. Phys. Chem. A* **2003**, *107*, 2943–2953.
(64) Shimoni-Livny, L.; Glusker, J. P.; Bock, W. *Inorg. Chem.* **1998**, *37*, 1853–1867.
(65) Hettich, R. L. *J. Am. Soc. Mass Spectrom.* **1999**, *10*, 941–949.
(66) Fridgen, T. D. *Mass Spectrom. Rev.* **2009**, *28*, 586–607.
(67) MacAleese, L.; Simon, A.; McMahon, T. B.; Ortega, J. M.; Scuderi, D.; Lemaire, J.; Maitre, P. *Int. J. Mass Spectrom.* **2006**, *249*, 14–20.
(68) Lemaire, J.; Boissel, P.; Heninger, M.; Mauclaire, G.; Bellec, G.; Mestdagh, H.; Simon, A.; Le Caer, S.; Ortega, J. M.; Glotin, F.; Maitre, P. *Phys. Rev. Lett.* **2002**, *89*, 273002–273001.
(69) Prell, J. S.; O'Brien, J. T.; Williams, E. R. *J. Am. Soc. Mass Spectrom.* **2010**, *21*, 800–809.
(70) Scuderi, D.; Correia, C. F.; Balaj, O. P.; Ohanessian, G.; Lemaire, J.; Maitre, P. *ChemPhysChem* **2009**, *10*, 1630–1641.
(71) Fridgen, T. D.; McMahon, T. B.; MacAleese, L.; Lemaire, J.; Maitre, P. *J. Phys. Chem. A* **2004**, *108*, 9008–9010.
(72) Oomens, J.; Sartakov, B. G.; Meijer, G.; von Helden, G. *Int. J. Mass Spectrom.* **2006**, *254*, 1–19.
(73) Armentrout, P. B.; Rodgers, M. T.; Oomens, J.; Steill, J. D. *J. Phys. Chem. A* **2008**, *112*, 2248–2257.
(74) Knobloch, B.; Sigel, H. *J. Biol. Inorg. Chem.* **2004**, *9*, 365–373.
(75) Salpin, J. Y.; Guillaumont, S.; Tortajada, J.; MacAleese, L.; Lemaire, J.; Maitre, P. *ChemPhysChem* **2007**, *8*, 2235–2244.
(76) Bakker, J. M.; Sinha, R. K.; Besson, T.; Brugnara, M.; Tosi, P.; Salpin, J.-Y.; Maitre, P. *J. Phys. Chem. A* **2008**, *112*, 12393–12400.
(77) Kryachko, E. S.; Nguyen, M. T.; Zeegers-Huyskens, T. *J. Phys. Chem. A* **2001**, *105*, 1934–1943.
(78) Hu, X.; Li, H.; Liang, W.; Shijun Han, S. *J. Phys. Chem. B* **2004**, *108*, 12999–12307.
(79) Topal, M. D.; Fresco, J. R. *Nature* **1976**, *263*, 285–289.
(80) Holbrook, S. R.; Cheong, C. J.; Tinoco, I.; Kim, S. H. *Nature* **1991**, *353*, 579–581.